

Thermal design method of bayonet-tube evaporators and condensers

N. Kayansayan

Dokuz Eylül University, Department of Mechanical Engineering, Bornova 35100,
 Izmir, Turkey

Received 23 March 1995; revised 26 September 1995

The paper describes an effectiveness-NTU design method of bayonet-tube evaporators and condensers. Including the effect of the wall superheat on the shell-side film coefficient, and using an energy balance on the tube, differential equations for the steady-state fluid temperatures are formulated. Because of the nonlinear nature of the governing equations, the fourth-order Runge–Kutta method is employed to the solution of the finite difference equations. The results are iterated with the combination of integration techniques. An upper bound to the numerical error being $\pm 5\%$, the fluid temperature distribution as well as the exchanger effectiveness are determined, and presented as a function of the Hurd number, the number of heat transfer units and the flow arrangement. For flow entering through the inner tube, the temperature distribution displays the occurrence of a minimum at a point other than the tube-tip of the exchanger. In an extension of the analysis, an effort is made to illustrate the deviation of the results obtained by uniform film coefficient from the present study, and the differences are outlined.

(Keywords: Heat exchanger; shell-and-tube exchanger; design; annular tube; condenser; evaporator; calculation)

Copyright © 1996 Published by Elsevier Science Ltd and IIR

Méthode de conception thermique d'évaporateurs et de condenseurs à tubes-baïonnettes

L'article décrit l'application aux évaporateurs et condenseurs à tubes à baïonnettes d'une méthode de conception par le nombre d'unités de transfert de chaleur (NTU), et son efficacité. En tenant compte de l'effet de la surchauffe de la paroi sur le coefficient du film côté calandre et en utilisant le bilan énergétique du tube, on établit des équations différentielles pour les températures du fluide en régime stable. A cause de la nature non linéaire des équations de base, on utilise la méthode Runge–Kutta du 4^e ordre pour résoudre les équations aux différences finies. Les résultats sont établis par itération et intégration. Avec une erreur numérique de + ou –5%, la distribution de température du fluide, ainsi que l'efficacité de l'échangeur, sont déterminées, et présentées en fonction du nombre de Hurd, du nombre d'unités de transfert de chaleur et de l'organisation des écoulements. Pour un flux entrant dans le tube intérieur, la distribution de température montre l'existence d'un minimum à un point autre que l'extrémité du tube de l'échangeur. En outre, on s'est efforcé d'illustrer l'écart des résultats obtenus par un coefficient de film uniforme, et on met en évidence les différences constatées.

(Mots clés: Echangeur de chaleur; échangeur multi-tubulaire; conception; tube annulaire; condenseur; évaporateur; calcul)

Copyright © 1996 Elsevier Science Ltd and IIR

A bayonet-tube exchanger consists of a pair of concentric tubes with a cap attached to the lower end of the outer tube. As shown in *Figure 1*, the essential feature of the exchanger is that the inner tubes, the outer tubes, and the shell are completely free to move independently from one another. The freely expanding elements greatly simplify the structure of the exchanger and eliminate the thermal stresses. The bayonet-tube is therefore particularly suited to extremely large temperature differentials between the two fluids and is excellently adapted to the evaporation or condensation of the shell-side fluid under moderate and very low vacuum conditions¹.

Contrary to the number of advantages of the bayonet-tube over conventional designs, the number of publica-

tions related to the subject is limited. The performance of the exchanger with the shell-side fluid flowing parallel to the tube axis was first analyzed by Hurd². Later, including the effect of radiative heat transfer between the inner and the outer tube surfaces and dividing the tube into N -slices, Chung^{3,4} numerically solved the heat transfer governing equations and determined the temperature distribution of the tube fluid. In his analysis, Chung^{3,4}, knowing the total convective and radiative heat transfer coefficient between the tubes of a particular slice, expressed the fluid temperatures in terms of the tube-wall temperatures, and solved the resulting $3N$ equations for temperatures by the Newton–Raphson method. Mathur *et al.*⁵ demonstrated an application

Nomenclature

A	Heat transfer surface area (m^2)
a	Ratio of the inside tube diameter to the outside
C_t	Tube parameter of evaporation ($\text{K}^{-7/3}$)
\bar{C}_t	Tube parameter of condensation ($\text{K}^{-3/4}$)
c_p	Specific heat at constant pressure ($\text{Jkg}^{-1} \text{K}^{-1}$)
d	Tube diameter (m)
F	Functions representing the wall superheat
Hu	Hurd number, Equation (19)
h	Heat transfer coefficient ($\text{Wm}^{-2} \text{K}^{-1}$)
k	Thermal conductivity ($\text{Wm}^{-1} \text{K}^{-1}$)
L	Tube length (m)
\dot{m}	Mass flowrate (kg s^{-1})
NTU_x	Local number of heat transfer units [$= h_m P_{01} x / \dot{m} c_p$]
NTU^*	Outer tube number of heat transfer units [$= h_m A_{01} / \dot{m} c_p$]
ntu	Inner tube number of heat transfer units [$= U_2 A_2 / \dot{m} c_p$]
P	Perimeter (m)
q	Heat-transfer rate (W)
R	Unit thermal resistance ($\text{m}^2 \text{KW}^{-1}$)
T	Temperature (K)
U	Overall heat-transfer coefficient ($\text{Wm}^{-2} \text{K}^{-1}$)
X	Nondimensional flow length [$= h_m P_{01} x / \dot{m} c_p$]
x	Flow length (m)

Greek letters

β	Condensation parameter ($\text{Wm}^{-2} \text{K}^{-3/4}$)
Δ	Difference
ε	Exchanger effectiveness
λ	Boiling parameter ($\text{W}^{3/10} \text{m}^{-3/5} \text{K}^{-1}$)
θ	Nondimensional temperature
ζ	Unit thermal resistance ratio

Subscripts

a	Analytical
e	Excess
ex	Exit
i	Internal
in	Inlet
j	Nodal point
max	Maximum
min	Minimum
o	External
s	Shell conditions
w	Wall
1	Annulus conditions
2	Inner tube conditions
*	Tube tip

Superscripts

-	Condenser
---	-----------

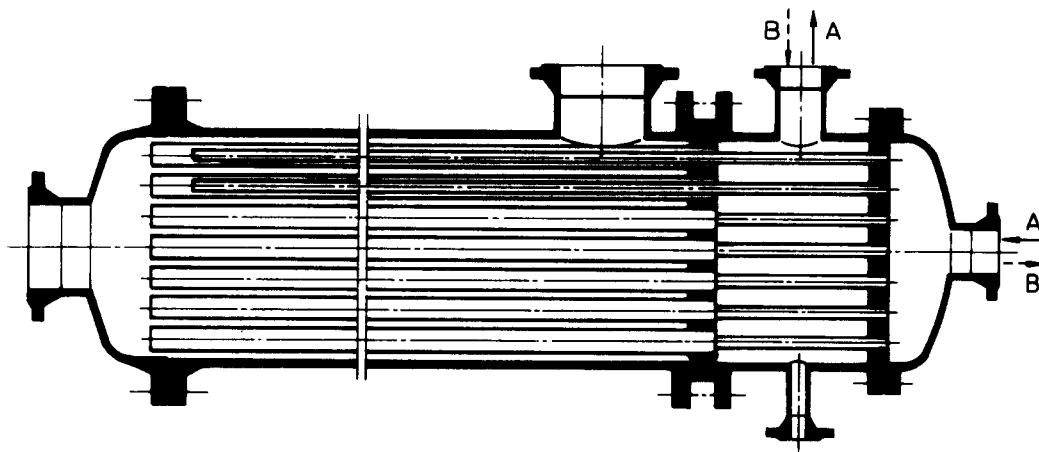


Figure 1 Schematic representation of bayonet-tube exchanger and the flow arrangements

Figure 1 Schéma d'un échangeur à tube à baïonnettes et disposition des écoulements

of the bayonet-tube as a heat-removing element in a fluidized bed system and a characteristic temperature difference was devised for calculating the bed-tube heat transfer rate. Luu and Grant⁶ investigated the effect of the flue gas temperature and the tube layout on the effectiveness of a ceramic bayonet-tube exchanger for recovering waste heat to preheat combustion air.

This work has been motivated principally by the lack of an effectiveness-NTU design method for the bayonet-tube evaporator and condenser operating under nonuniform heat transfer conditions along the outer tube surface. Accounting for the strong dependence of the shell-side film coefficient on the wall excess temperature, an

algorithm is developed for solving the basic governing equations of the exchanger. In predicting the thermal behaviour of the bayonet-tube, the parameters that affect the design are characterized.

As illustrated in Figure 1, the tube-side fluid might enter the exchanger through the inner tube and exit through the annulus. This flow arrangement is identified as path A, and the reverse flow as path B. Thus, depending upon the flow path of the tube-side fluid, four different configurations are to be examined. In turn, two for evaporation and two for condensing conditions are studied. For all cases, the dependence of the outer-tube outer-surface heat-transfer coefficient on the wall excess

temperature; $\Delta T_e = \pm(T_w - T_s)$, is taken into account. In the analysis, steady-state flow conditions are assumed to exist. The nondimensional governing equations indicated that besides the flow arrangement, three independent parameters, namely the local number of heat transfer units, NTU_x , the Hurd number, Hu , and the ratio of the unit heat transfer resistance of the annulus fluid to the resistance of the phase changing fluid, ζ , affect the temperature variations in the exchanger. For given values of Hu and ζ out of the range $0 \leq Hu \leq 5$ and $10^{-5} \leq \zeta \leq 10^{-1}$ the number of heat transfer units of the outer tube surface, $NTU^* = h_m A_{o1} / mc_p$, is determined by satisfying the thermal conditions at the tube-tip, and is found to vary from 0.028 to 9.655 in the analysis. The Hurd number, defined as the ratio of the number of heat transfer units of the inner tube to the outer, $Hu = ntu / NTU^*$, spanned the range from 0 to 5. Hence, the methodology and the diagrams presented are directly applicable to the design of bayonet-tube evaporators and condensers.

Formulation of the model and the solution method

In the derivation of the governing equations, to reduce the dimensionality of the problem, the fluid temperature at a particular tube cross-section is represented by a mean value, and the heat conduction in the axial direction is neglected in comparison with the heat convection in the radial direction. The flow conditions in the inner tube and the annulus are assumed to be fully developed. Then the related heat-transfer coefficients are uniform along the flow path and, for specified flow parameters, may be determined by the duct flow correlations published in the open literature⁷. Pertaining to the present application of the bayonet-tube, since the ratio of the temperature change of the tube-side fluid to the shell-side temperature, $\Delta T / T_s$, is much less than unity, the thermal properties of the tube-side fluid are assumed to be constant and are evaluated at the mean value of the inlet and the exit temperatures. The heat-transfer rate at the sealed end, $x = L$, is negligibly small in comparison with the overall heat transfer rate of the exchanger. Hence, the inner tube and the annulus fluid temperatures are assumed to be identical at $x = L$. This boundary condition also implies that the total heat rate transferred

through the exchanger may be computed by the energy balance along the outer surface of the outer tube.

Evaporator

As depicted in Figure 2, together with the above stated assumptions, employing the energy balance equation to a differential control volume yields:

$$\text{inner tube: } \dot{m}c_p \frac{dT_2}{dx} \pm U_2 P_2 (T_2 - T_1) = 0 \quad (1)$$

$$\text{annulus: } \dot{m}c_p \frac{dT_1}{dx} \pm [U_2 P_2 (T_2 - T_1) - U_1 P_1 (T_1 - T_s)] = 0 \quad (2)$$

where the plus and the minus signs are to be respectively employed for the flow arrangements A and B. The temperature related boundary conditions are:

$$\text{at } x = 0, \quad T_k = T_{in} \quad (3)$$

$$\text{and, at } x = L, \quad T_1 = T_2 \quad (4)$$

In Equation (3), the subscript k assumes the value of 2 for the flow path A, and 1 for the reverse flow. The equality of temperatures at $x = L$ also satisfies the condition of insulated tube-tip through Equation (1). Furthermore, the overall energy balance on the outer tube surface is:

$$q = \dot{m}c_p (T_{in} - T_{ex}) = \int_{x=0}^L h_{o1} P_{o1} (T_w - T_s) dx \quad (5)$$

In Equations (1) and (2), U_2 represents the overall heat-transfer coefficient between the inner tube fluid and the annulus, and is assumed to be constant along the flow direction. However, with respect to the shell-side tube surface, the overall heat-transfer coefficient of the outer tube may be expressed as,

$$\frac{1}{U_1} = R_1 + \frac{1}{h_{o1}} \quad (6)$$

where the thermal resistance per unit surface area, R_1 , is defined as follows:

$$R_1 = \frac{1}{ah_{i1}} + \frac{R_{di}}{a} + R_{do} + \frac{d_{o1}}{2k_w} \ln \frac{d_{o1}}{d_{i1}} \quad (7)$$

Here, a is the ratio of the inside to the outside diameters of the outer tube and is assumed to be 0.85 in the analysis. With regard to the type of fluids in use, the fouling factors R_{di} and R_{do} in Equation (7) may be estimated through TEMA standards⁸ for practical design purposes.

In the nucleate pool boiling regime, the film coefficient with respect to the outer surface of the outer tube, h_{o1} , is proportional to the seven-thirds power of the wall excess temperature, ΔT_e , and small changes in the wall temperature drastically modify the film coefficient⁹. In the analysis, therefore, h_{o1} is expressed as:

$$h_{o1} = \lambda^{10/3} \Delta T_e^{7/3} \quad (8)$$

Besides Equations (1) and (2), the functional dependence of h_{o1} on ΔT_e necessitates one additional relation for analysing the temperature fields T_w , T_1 and T_2 of the exchanger. Referring to the results of Kayansayan¹⁰, the temperatures of the annulus fluid and the outer tube

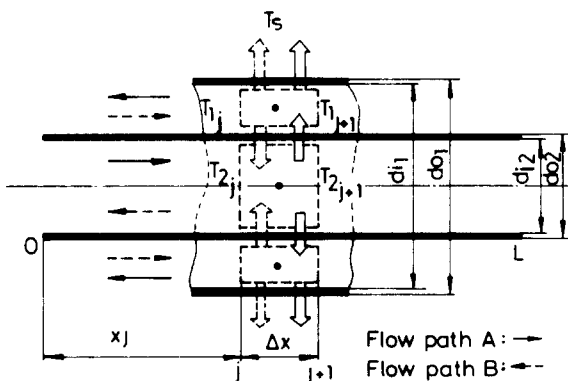


Figure 2 Thermal energy balance around a tube section for evaporator analysis

Figure 2 Bilan énergétique thermique autour d'une section de tube, pour l'analyse de l'évaporateur

wall may be related as:

$$T_1 - T_s = C_t(T_w - T_s)^{10/3} + (T_w - T_s) \quad (9)$$

where the tube parameter C_t is:

$$C_t = \frac{\lambda^{10/3} R_1}{a} \quad (10)$$

Moreover the temperatures and the flow length are non-dimensionalized and expressed as follows,

$$\theta_1 = \frac{T_1 - T_s}{T_{in} - T_s}, \quad \theta_2 = \frac{T_2 - T_s}{T_{in} - T_s}, \quad \theta_e = \frac{T_w - T_s}{T_{in} - T_s} \quad (11)$$

and

$$X = \frac{h_m P_{o1}}{\dot{m} c_p} X \quad (12)$$

It has to be noted that the nondimensional flow length, X , is identical with the local number of heat transfer units, NTU_X , and h_m is a fictitious boiling film coefficient evaluated at the exchanger maximum temperature difference as:

$$h_m = \lambda^{10/3} (T_{in} - T_s)^{7/3} \quad (13)$$

Thus the nondimensional form of h_{o1} is:

$$\frac{h_{o1}}{h_m} = \theta_e^{7/3} \quad (14)$$

Substituting Equation (8) into (6) and together with Equation (9), Equations (1) and (2) are rearranged and transformed into nondimensional form through Equations (11), (12) and (14). Further mathematical manipulations resulted, with the following nonlinear and coupled differential equations for temperatures θ_2 and θ_e :

$$\frac{d\theta_2}{dX} = \pm [\text{Hu}(\theta_e F2 - \theta_2)] \quad (15)$$

$$\frac{d\theta_e}{dX} = \pm \left[\left(\frac{\text{Hu}F1 + \theta_e^{7/3} F2}{F4} \right) \theta_e - \left(\frac{\text{Hu}F3}{F4} \right) \theta_2 \right] \quad (16)$$

and

$$\theta_1 = \theta_e + \zeta \theta_e^{10/3} \quad (17)$$

where ζ is the outer tube thermal resistance ratio, and through Equations (10) and (13), is defined as:

$$\zeta = \frac{R_1}{a/h_m} \quad (18)$$

and the Hurd number is determined by:

$$\text{Hu} = \frac{\text{ntu}}{\text{NTU}_*} \quad (19)$$

Consequently the non-dimensional boundary conditions are:

$$\text{at } X = 0, \quad \theta_k = 1 \quad (20)$$

$$\text{at } X_* = \frac{h_m P_{o1}}{\dot{m} c_p} L = \text{NTU}_*, \quad \theta_1 = \theta_2 \quad (21)$$

and Equation (5) provides the exchanger outlet temperature as:

$$\theta_p(0) = 1 - \int_{X=0}^{\text{NTU}_*} \theta_e^{10/3} dX \quad (22)$$

where the subscript p assumes the value of 1 for the flow arrangement A and 2 for the reverse flow case. In Equations (15) and (16), the F -functions are functions of the wall excess temperature and are stated to be:

$$F1 = 1 + (1 + a)\zeta\theta_e^{7/3} + a\zeta^2\theta_e^{14/3} \quad (23)$$

$$F2 = 1 + \zeta\theta_e^{7/3} \quad (24)$$

$$F3 = 1 + a\zeta\theta_e^{7/3} \quad (25)$$

$$F4 = 1 + \left(\frac{10}{3} + a\right)\zeta\theta_e^{7/3} + \frac{10}{3}a\zeta^2\theta_e^{14/3} \quad (26)$$

In numerical analysis, the location of a particular nodal point j with respect to the exchanger inlet is calculated as,

$$X_j = (j - 1)\Delta X = \text{NTU}_j \quad (27)$$

The increment size, ΔX , is assumed to be 0.001, and $j = 1$ corresponds to the exchanger inlet.

To provide a solution to the temperature fields, first the unit thermal resistance ratio, ζ , and the Hurd number, Hu , of a particular exchanger have to be specified and supplied as input data. Then the flow arrangement is selected. For flow arrangement A, the value of θ_1 at $j = 1$ is assumed, and through the application of the Newton-Raphson method of iteration, Equation (17) is solved for the corresponding θ_e -value at $j = 1$. Together with the initial values of θ_e and θ_2 , and the F -functions evaluated at $j = 1$, then Equations (15) and (16) are integrated simultaneously using the fourth-order Runge-Kutta scheme¹¹ and the temperatures at an adjacent point $j + 1$ are determined. In turn the annulus fluid temperature at $j + 1$ is computed by substituting $(\theta_e)_{j+1}$ into Equation (17). The resolution of temperatures along the flow is progressively continued until the following condition is satisfied,

$$\text{at } j = j^*, \quad |\theta_1 - \theta_2| < 5 \times 10^{-4} \quad (28)$$

Next, Simpson's one-third rule of integration is applied to Equation (22) for determining the new value of θ_1 at $j = 1$. The algorithm proceeds with the comparison of the new and the old values of $(\theta_1)_{j=1}$, and if $|\theta_{1,\text{new}} - \theta_{1,\text{old}}|_{j=1}$ is less than 5×10^{-4} , the computation terminates. Otherwise the computational scheme is repeated with the recently determined value of $(\theta_1)_{j=1}$. Satisfying the energy balance condition, the program terminates with a graphical illustration of the three temperature distributions, and provides the location and the value of the minimum temperature of the fluid flowing through the bayonet-tube. The exchanger effectiveness and the NTU_* -value are also computed for the specified design conditions.

For the reverse flow case, as indicated by the dashed line in *Figure 2*, the algorithm employed slightly differs from the previous analysis in the sense that the value of $(\theta_1)_{j=1}$ computed for the flow arrangement A is assumed to be $(\theta_2)_{j=1}$ for the flow arrangement B at identical parameters of Hu and ζ . Then, at the lower end of the tube, satisfying the condition stated by Equation (28), the value of j^* , and through Equation (27) the corresponding value of NTU_* are estimated. Finally, evaluating Equation (22) for $p = 2$, the energy balance requirement is checked by the same numerical integration technique. Thus the method of solution provides a basis for illustrating the effect of the flow arrangement

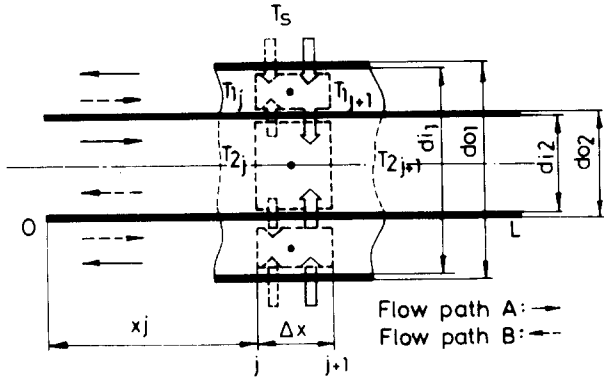


Figure 3 Thermal energy balance around a tube section for condenser analysis

Figure 3 *Bilan énergétique thermique autour d'une section de tube, pour l'analyse du condenseur*

on the thermal behaviour of the exchanger at identical design conditions.

Condenser

A similar method of analysis may be employed to the differential control volume in *Figure 3* to yield the governing equations of condensation as follows:

$$\text{Inner tube: } \dot{m}c_p \frac{dT_2}{dx} \pm U_2 P_2 (\bar{T}_2 - \bar{T}_1) = 0 \quad (29)$$

$$\begin{aligned} \text{Annulus: } \dot{m}c_p \frac{dT_1}{dx} \pm [U_2 P_2 (\bar{T}_2 - \bar{T}_1) \\ + U_1 P_1 (T_s - \bar{T}_1)] = 0 \end{aligned} \quad (30)$$

and the boundary conditions expressed in Equations (3), (4) and (5) are equally applicable to the present problem.

Convective film condensation is assumed to occur on the outer tube surface, and the heat-transfer coefficient averaged over the tube circumference is¹²:

$$\bar{h}_{o1} = \beta(\Delta T_e)^{-1/4} \quad (31)$$

where β depends upon the thermo-physical properties of the condensing vapour and the tube diameter d_{o1} . Similar to the method followed in the evaporator analysis, the annulus fluid and the outer tube wall temperatures are related as follows:

$$T_s - \bar{T}_1 = \bar{C}_1 (T_s - \bar{T}_w)^{3/4} + (T_s - \bar{T}_w) \quad (32)$$

where \bar{C}_1 is the tube parameter of condensation and is expressed as:

$$\bar{C}_1 = \frac{\beta R_1}{a} \quad (33)$$

The nondimensional temperatures are represented as,

$$\bar{\theta}_1 = \frac{T_s - \bar{T}_1}{T_s - T_{in}}, \quad \bar{\theta}_2 = \frac{T_s - \bar{T}_2}{T_s - T_{in}}, \quad \bar{\theta}_e = \frac{T_s - \bar{T}_w}{T_s - T_{in}} \quad (34)$$

and the nondimensional flow length is as in Equation (12). Furthermore, the outer tube film coefficient becomes:

$$\frac{\bar{h}_{o1}}{h_m} = \bar{\theta}_e^{-1/4} \quad (35)$$

In condensation, it has to be noted that an increase in $\bar{\theta}_e$ causes a decrease in the outer tube surface conductance. In Equation (35), h_m presents a fictitious film coefficient evaluated at the maximum temperature difference of the exchanger as following:

$$\bar{h}_m = \beta(T_s - T_{in})^{-1/4} \quad (36)$$

Rearranging Equation (6) in terms of \bar{h}_{o1} as given by Equation (35), and then substituting U_1 into Equation (30), the governing equations may be reduced to the following nondimensional form:

$$\frac{d\bar{\theta}_2}{dX} = \pm [\bar{H}u(\bar{\theta}_e^{3/4} F6 - \bar{\theta}_2)] \quad (37)$$

$$\frac{d\bar{\theta}_e}{dX} = \pm \left[\left(\frac{\bar{H}u F5 + F6}{F8} \right) \bar{\theta}_e - \left(\frac{\bar{H}u F7}{F8} \right) \bar{\theta}_e^{1/4} \bar{\theta}_2 \right] \quad (38)$$

$$\bar{\theta}_1 = \bar{\theta}_e + \bar{\zeta} \bar{\theta}_e^{3/4} \quad (39)$$

where $\bar{\zeta}$ is the outer tube thermal resistance ratio, and is defined as in Equation (18).

In Equations (37) and (38), the plus and the minus signs are to be used respectively for the flow arrangements A and B. In expressing the appropriate boundary conditions for the present problem, similar to the evaporator analysis, the subscript k in Equation (20) becomes 2 for the flow path A and 1 for the reverse flow. However, h_m in Equation (21), has to be replaced with \bar{h}_m . The energy integral equation, Equation (5), is modified and transformed into a nondimensional form through the use of Equation (35). Then the exchanger outlet temperature of the tube-side fluid is:

$$\bar{\theta}_p(0) = 1 - \int_{X=0}^{\overline{NTU}_*} \bar{\theta}_e^{3/4} dX \quad (40)$$

Finally the F -functions in Equations (37) and (38) are determined to be as follows,

$$F5 = a\bar{\zeta}^2 + (1+a)\bar{\zeta}\bar{\theta}_e^{1/4} + \bar{\theta}_e^{1/2} \quad (41)$$

$$F6 = \bar{\zeta} + \bar{\theta}_e^{1/4} \quad (42)$$

$$F7 = a\bar{\zeta} + \bar{\theta}_e^{1/4} \quad (43)$$

$$F8 = \frac{3}{4}a\bar{\zeta}^2 + (\frac{3}{4}+a)\bar{\zeta}\bar{\theta}_e^{1/4} + \bar{\theta}_e^{1/2} \quad (44)$$

Due to substantial difference in heat-transfer mechanism, there is no similarity between the evaporator and the condenser F -functions. However, a similar algorithm may be followed in determining the \overline{NTU}_* , the location and the value of the minimum temperature in the tube, and the exchanger effectiveness at a particular design condition. In the condenser computations, the algorithm also provides the temperature distribution patterns of the tube-side fluid for both flow arrangements.

Results and discussion

Evaporator

In regard to the nondimensional governing equations, the temperature of the tube-side fluid is a function of four independent parameters, and the functional dependence may be stated as:

$$\theta = \theta(\overline{NTU}_*, \bar{H}u, \bar{\zeta}, \text{Flow arrangement}) \quad (45)$$

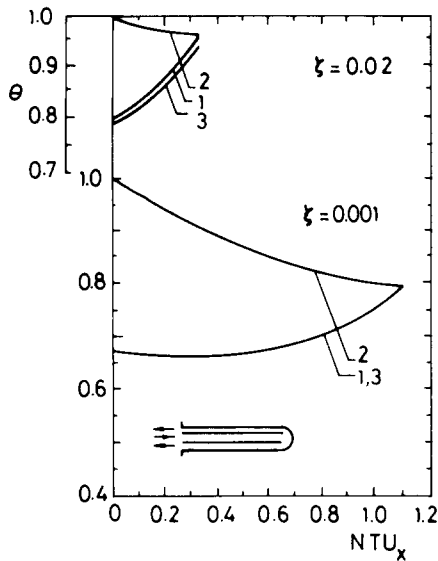


Figure 4 Evaporator temperature distribution for flow arrangement A at $Hu = 1.0$. (1) θ_1 , (2) θ_2 , (3) θ_e
 Figure 4 *Distribution de la température à l'évaporateur pour la disposition des écoulements A, avec $Hu = 1.0$. (1) θ_1 , (2) θ_2 , (3) θ_e*

Thus applying the solution method to the aforementioned relations yields the temperature distributions along the exchanger. The typical temperature patterns of the flow arrangement A at $Hu = 1$ are depicted in Figure 4. At a large value of ζ (i.e. $\zeta = 0.02$) which corresponds to a case with a high thermal resistance on the annular side, the difference in temperatures θ_1 , and θ_e are distinguishable. However, as ζ decreases, these two temperatures nearly coincide and an increase in NTU^* -value is noticed. At a fixed value of the boiling film coefficient, h_m , the decrease in ζ might be due to relative decrease in the thermal resistance of the annulus fluid. This in turn causes the outer tube energy balance requirement to be sufficed at a larger value of NTU^* for a particular Hurd

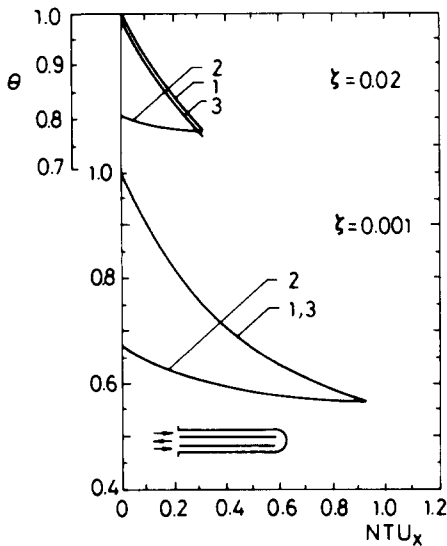


Figure 5 Evaporator temperature distribution for the reversed flow at $Hu = 1.0$. (1) θ_1 , (2) θ_2 , (3) θ_e
 Figure 5 *Distribution de la température à l'évaporateur pour l'écoulement inversé avec $Hu = 1.0$. (1) θ_1 , (2) θ_2 , (3) θ_e*

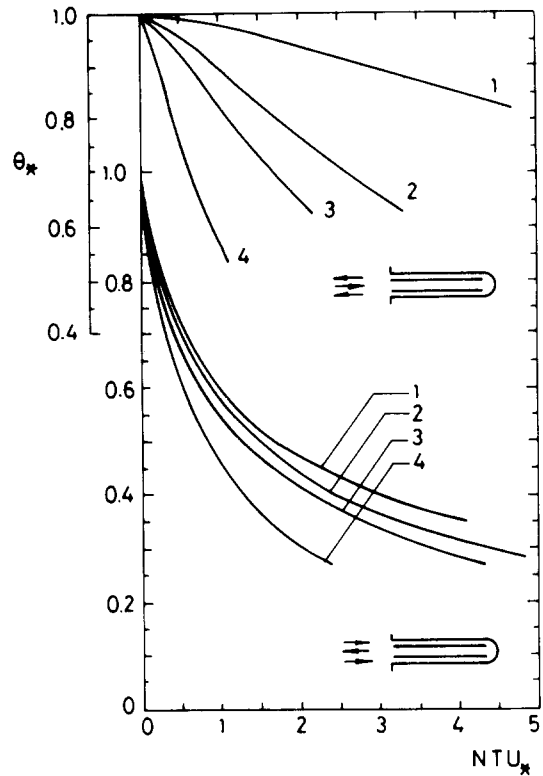


Figure 6 Variation of evaporator tube-tip temperature. The upper curves are for the flow path A, and the lower ones are for path B. Hu : (1) 0.1, (2) 0.5, (3) 1.0, (4) 5.0
 Figure 6 *Variation de la température du tube de l'évaporateur. Les courbes supérieures correspondent à l'écoulement A, et les courbes inférieures correspondent à l'écoulement B. Hu : (1) 0.1, (2) 0.5, (3) 1.0, (4) 5.0*

number. As can be seen from Figure 4, the decrease in ζ also alters the typical trend of temperature distributions. The decay in θ_2 becomes stronger, and the occurrence of a minimum in the temperature distribution of the tube-side fluid is noticed. At the downstream position of this minimum, the increase in temperature indicates that a certain amount of heat energy supplied through the inner tube is regained by the fluid in the annulus.

To provide a comparison for the sole effect of reversing the flow on the thermal behaviour of the bayonet-tube evaporator the temperature patterns for the reverse flow at conditions identical with the previous case are displayed in Figure 5. Owing to the inlet of high temperature fluid through the annulus, the higher wall excess temperatures may result with higher heat flowrates on the outer tube surface. Then the overall energy balance is sustained at smaller NTU^* values. As ζ decreases, the difference in NTU^* values computed for both flow arrangements increases, and the effect of reversing the flow becomes stronger. As shown in Figure 5, the typical trend of θ_2 is to increase along the flow and the minimum fluid temperature always occurs at the tube-tip.

The determination of the tip temperature plays an important role in controlling the temperature drop of the tube-side fluid. Since the tip conditions are identified at $x = L$, the tip temperature then becomes only a function of Hu and NTU^* . This functional dependence on NTU^* for both flow arrangements and for $Hu = 0.1, 0.5, 1.0$ and 5.0 is illustrated in Figure 6. The general trend of θ^* is to decline as NTU^* increases. Due to relative increase in

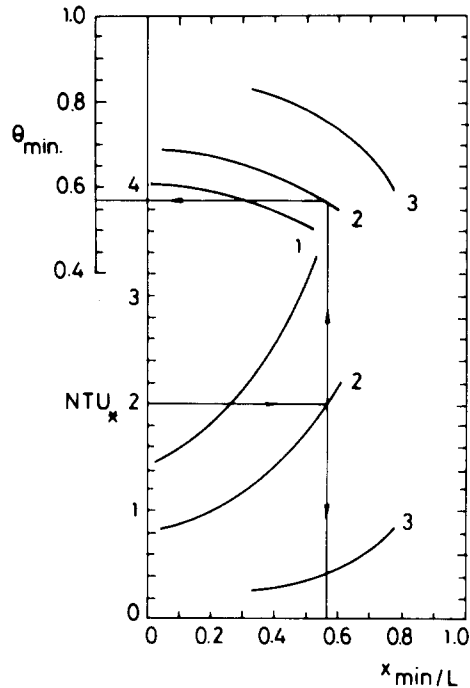


Figure 7 The position and the value of the minimum temperature for evaporator. Hu: (1) 0.5, (2) 1.0, (3) 5.0

Figure 7 Position et valeur de la température minimale pour l'évaporateur. Hu: (1) 0.5, (2) 1.0, (3) 5.0

the inner tube number of heat transfer units, ntu , as Hu -number increases, the decay in the tip temperature becomes steeper. The effect of the flow arrangement on the tip temperature might be revealed by comparing the values of θ^* at a particular NTU^* and Hu number. The existence of a drastic drop in θ^* for the reverse flow is in accord with high heat-transfer rates on the outer tube surface.

The location and the numerical value of the minimum temperature that occurs for flow arrangement A might be critical at a decision-making stage for certain applications. Hence these parameters should be made available to the designer, and the chart presented in *Figure 7* may be used for this purpose. In this figure, x_{min} indicates the location of the minimum temperature from the inlet of the exchanger, and for predetermined parameters of NTU^* and Hu , the first set of curves provides x_{min}/L and then the curves above yield the corresponding minimum fluid temperature. It is evident from *Figure 7* that at a particular Hu -number, there exists a specific value of NTU^* for which $x_{min}/L = 0$ and $(\theta)_{min}$ represents the exchanger outlet temperature. At a particular NTU^* , however, an increase in Hu causes the location of $(\theta)_{min}$ to move toward the tube-tip, and the minimum temperature numerically increases.

In assessing the performance of an exchanger, the effectiveness plays an important role in the thermal design. For the present study, analysing the functional dependence and the variation of the effectiveness is a prime factor in describing the thermal behaviour of the bayonet-tube evaporator. Due to phase-change in the shell, the tube-side fluid has the minimum heat capacity rate, and the conventional definition of the effectiveness yields:

$$\varepsilon = \frac{q}{q_{max}} = 1 - (\theta_p)_{j=1} \quad (46)$$

Where $(\theta_p)_{j=1}$ is the outlet temperature of the tube fluid

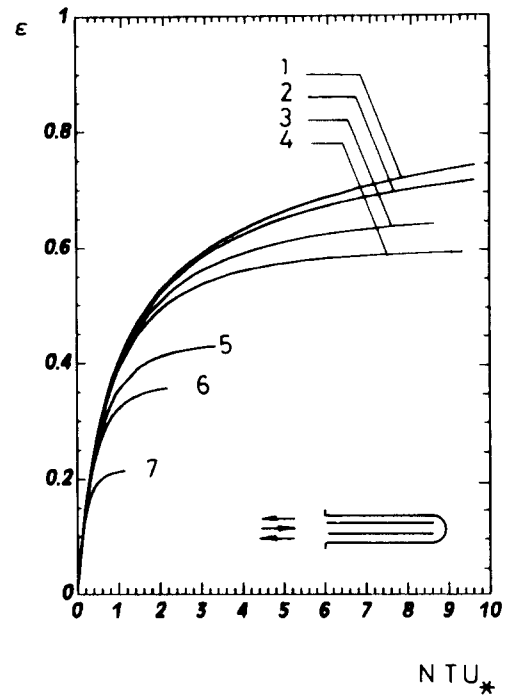


Figure 8 Evaporator effectiveness for flow arrangement A. Hu: (1) 0.0, (2) 0.01, (3) 0.05, (4) 0.1, (5) 0.5, (6) 1.0, (7) 5.0

Figure 8 Efficacité de l'évaporateur pour l'écoulement A. Hu: (1) 0.0, (2) 0.01, (3) 0.05, (4) 0.1, (5) 0.5, (6) 1.0, (7) 5.0

and the subscript p is 1 for flow arrangement A and 2 for the reverse flow. The dependence of ε on the outlet temperature indicates the functional form to be as follows:

$$\varepsilon = \varepsilon(NTU^*, Hu, \text{Flow arrangement}) \quad (47)$$

In the design of the bayonet-tube evaporator for a particular heat duty, then the values of NTU^* and Hu have to be predetermined. Then the variation of ε with respect to NTU^* for a particular Hu -number might be obtained. *Figures 8* and *9* illustrate the effectiveness results as a function of NTU^* for flow arrangements A and B respectively, and for $Hu = 0.0, 0.01, 0.05, 0.1, 0.5, 1.0, 5.0$. In these figures, the condition for which $Hu = 0$ corresponds to a case with no heat interaction between the inner-tube and the annulus and the bayonet-tube behaves like a single tube. Hence, the effectiveness distributions for both flow arrangements are identical at $Hu = 0$. However, for $Hu > 0$, the deviation in effectiveness due to flow arrangement becomes distinct. Evidently, the reversed flow enhances the exchanger performance by providing as high as 10% increase in the exchanger effectiveness.

As can be noticed from *Figures 8* and *9*, the increase of Hu -number results with a smaller solution domain for the exchanger effectiveness. To provide high values of Hu , the parameter NTU^* should be decreased. This, in turn, may physically be accomplished by decreasing the surface area A_{o1} for identical values of ζ and inlet conditions. In fact, for infinitely large values of Hu , the condition of zero heat transfer rate to the shell-side fluid at a particular ζ -value necessitates the surface area A_{o1} to be zero. As a consequence, the solution domain disappears as Hu approaches infinity.

Condenser

In a manner similar to evaporator analysis, *Figure 10*

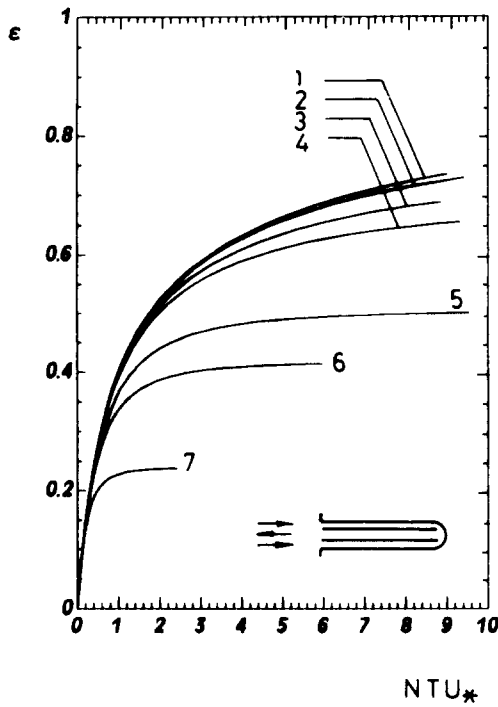


Figure 9 Evaporator effectiveness for flow arrangement B. Hu : (1) 0.0, (2) 0.01, (3) 0.05, (4) 0.1, (5) 0.5, (6) 1.0, (7) 5.0

Figure 9 Efficacité de l'évaporateur pour l'écoulement B. Hu : (1) 0.0, (2) 0.01, (3) 0.05, (4) 0.1, (5) 0.5, (6) 1.0, (7) 5.0

illustrates the typical temperature distribution patterns for the flow arrangement A at $\bar{\zeta} = 0.01$ and 0.001. For both flow conditions, the \overline{Hu} -number is assumed to be constant at $\overline{Hu} = 1.0$. A decrease in $\bar{\zeta}$ enhances the

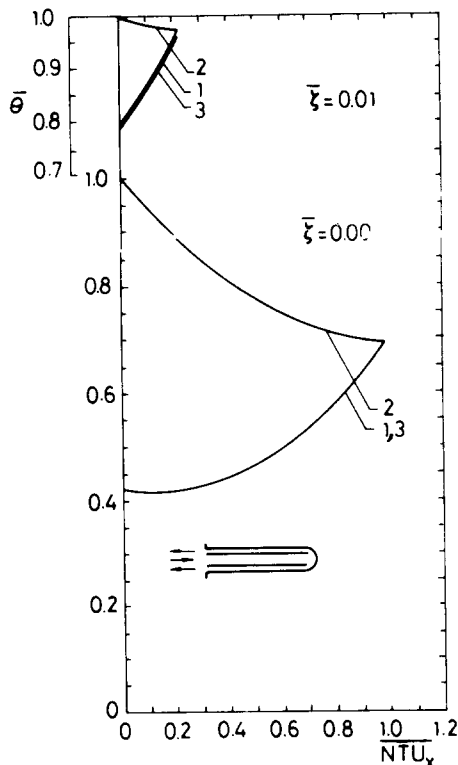


Figure 10 Condenser temperature distribution for flow arrangement A at $\overline{Hu} = 1.0$. (1) $\bar{\theta}_1$, (2) $\bar{\theta}_2$, (3) $\bar{\theta}_c$

Figure 10 Distribution de la température du condenseur pour l'écoulement A, avec $Hu = 1.0$. (1) $\bar{\theta}_1$, (2) $\bar{\theta}_2$, (3) $\bar{\theta}_c$

heat-transfer conductance of the fluid in the annulus and a greater value of \overline{NTU}_* results. Moreover, the temperature distribution in the inner tube becomes steeper and the fluid exits at a lower temperature. As can be seen from Figure 10, at $\bar{\zeta} = 0.001$, the temperature curve of the annulus fluid passes through a minimum.

To identify the effect of flow reversal on the thermal behaviour of the exchanger, the temperature patterns for flow arrangement B at identical design conditions with the previous case are depicted in Figure 11. Contrary to the evaporator analysis, as $\bar{\zeta}$ decreases, an increase in \overline{NTU}_* relative to flow arrangement A is noticed. This behaviour of condensation is attributed to the occurrence of higher wall excess temperature as the low-temperature fluid enters the exchanger through the annulus. Thus a reduction in the heat-transfer coefficient takes place. Then to provide the same performance as the flow arrangement A, the decrease in the film coefficient is compensated by an increase in the outer tube surface area. As a result, \overline{NTU}_* increases. The decrease in $\bar{\zeta}$ also causes the difference between $\bar{\theta}_c$ and $\bar{\theta}_1$ to become indistinguishable in Figure 11.

The variation of the tube-tip temperature of the condenser for both flow arrangements and for $\overline{Hu} = 0.1, 0.5, 1.0, 5.0$ is shown in Figure 12. Owing to the mitigation of the inner tube conductance relative to the outer tube as \overline{Hu} increases, a decrease in $\bar{\theta}_*$ is noted for a particular value of \overline{NTU}_* . As can be seen from this figure, at large values of \overline{Hu} (i.e. $\overline{Hu} = 5$), $\bar{\theta}_*$ approaches zero as \overline{NTU}_* approaches unity, and the difference between the temperatures of the tube and the shell fluids at the tip becomes negligibly small. As displayed in Figure 12, the effect of the flow reversal on the tip temperature is to increase the slope of the $\bar{\theta}_*$ -curve.

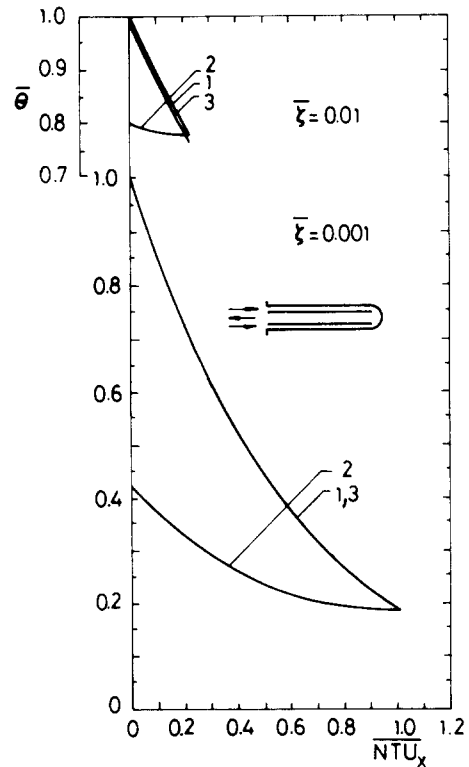


Figure 11 Condenser temperature distribution for the reversed flow at $\overline{Hu} = 1.0$. (1) $\bar{\theta}_1$, (2) $\bar{\theta}_2$, (3) $\bar{\theta}_c$

Figure 11 Distribution de la température du condenseur pour l'écoulement inversé, avec $Hu = 1.0$. (1) $\bar{\theta}_1$, (2) $\bar{\theta}_2$, (3) $\bar{\theta}_c$

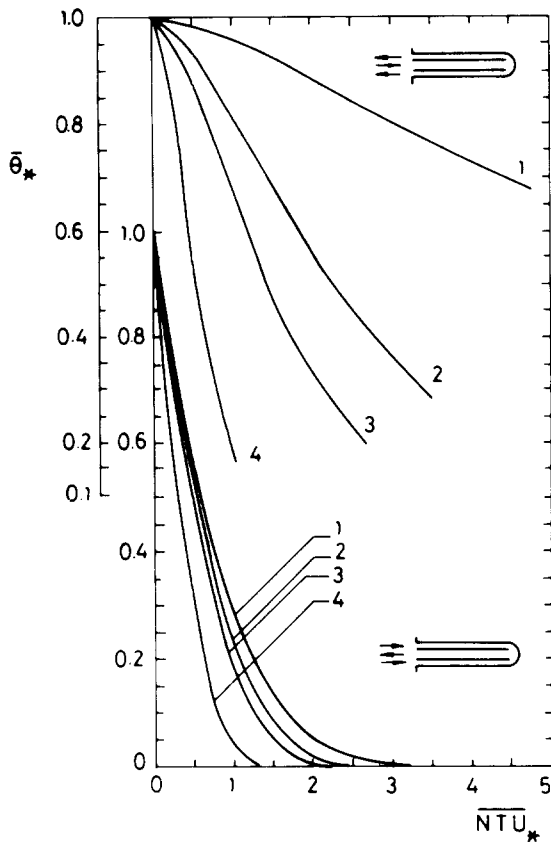


Figure 12 Variation of condenser tube-tip temperature. The upper curves are for flow path A, and the lower ones are for path B. \overline{Hu} : (1) 0.1, (2) 0.5, (3) 1.0, (4) 5.0

Figure 12 *Variation de la température du tube du condenseur. Les courbes supérieures correspondent à l'écoulement A, et les courbes inférieures correspondent à l'écoulement B. \overline{Hu} : (1) 0.1, (2) 0.5, (3) 1.0, (4) 5.0*

In contrast to the thermal behaviour of the evaporator, the temperature distribution of the tube-side fluid exhibits a maximum for flow arrangement A. It has to be noted that the maximum of \overline{T}_1 in the actual temperature scale corresponds to the minimum of $\bar{\theta}_1$ in the non-dimensional scale. Considering the significance of this minimum in the thermal design, the chart presented in Figure 13 may be used for locating and determining the $(\bar{\theta})_{\min}$. At a specified \overline{Hu} -number, there exists a particular value of \overline{NTU}_* for which $(\bar{\theta})_{\min}$ coincides with the exchanger outlet temperature. As \overline{NTU}_* increases, however, the location of $(\bar{\theta})_{\min}$ moves toward the tube-tip. Especially at large values of \overline{Hu} , the increase in x_{\min}/L causes a sharp decay in $(\bar{\theta})_{\min}$ and this is considered to be a distinctive behaviour of the condenser.

The implication of Equation (46) to the results of the bayonet-tube condenser yields the exchanger effectiveness and Figures 14 and 15, respectively, present ϵ vs \overline{NTU}_* behaviour for flow arrangements A and B at the parameterized values of $\overline{Hu} = 0.0, 0.05, 0.1, 0.5, 1.0, 5.0$. As can be seen from these figures, the slope of the ϵ vs \overline{NTU}_* curve is much steeper than the case of the evaporator, and the effectiveness approaches a maximum at smaller values of \overline{NTU}_* . Due to single tube behaviour at $\overline{Hu} = 0.0$, no appreciable change in ϵ is observed on reversing the flow. However, for $\overline{Hu} > 0$, because of the inverse proportionality between the condensate film coefficient and the one-fourth power

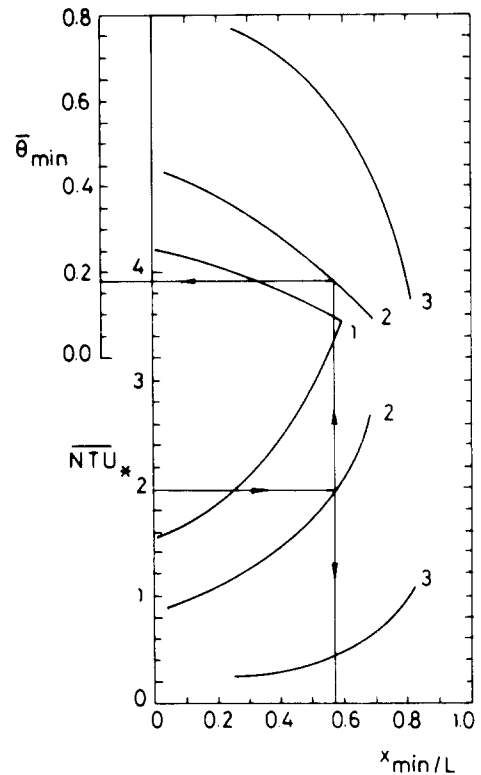


Figure 13 The position and the value of the minimum temperature for condenser. \overline{Hu} : (1) 0.5, (2) 1.0, (3) 5.0

Figure 13 *Position et valeur de la température minimale pour le condenseur. \overline{Hu} : (1) 0.5, (2) 1.0, (3) 5.0*

of the wall excess temperature, the difference in ϵ s computed for both flow arrangements at identical conditions increases as \overline{NTU}_* increases. Evidently, a condenser with the flow arrangement A provides as high as 5% increase in the exchanger performance.

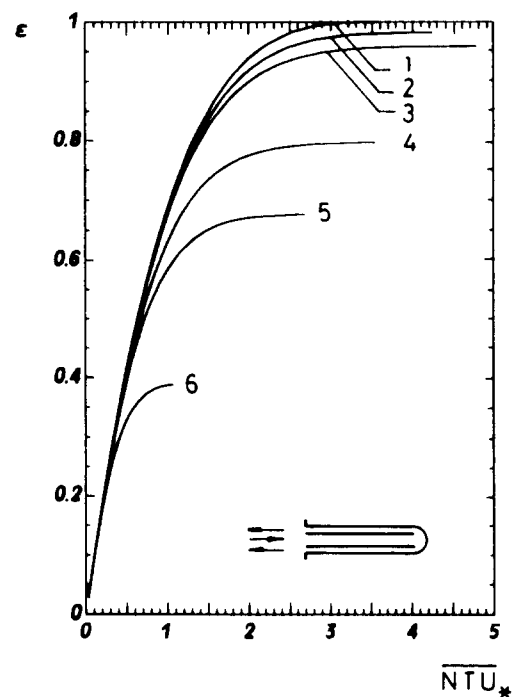


Figure 14 Condenser effectiveness for flow arrangement A. \overline{Hu} : (1) 0.0, (2) 0.05, (3) 0.1, (4) 0.5, (5) 1.0, (6) 5.0

Figure 14 *Efficacité du condenseur pour l'écoulement A. \overline{Hu} : (1) 0.0, (2) 0.05, (3) 0.1, (4) 0.5, (5) 1.0, (6) 5.0*

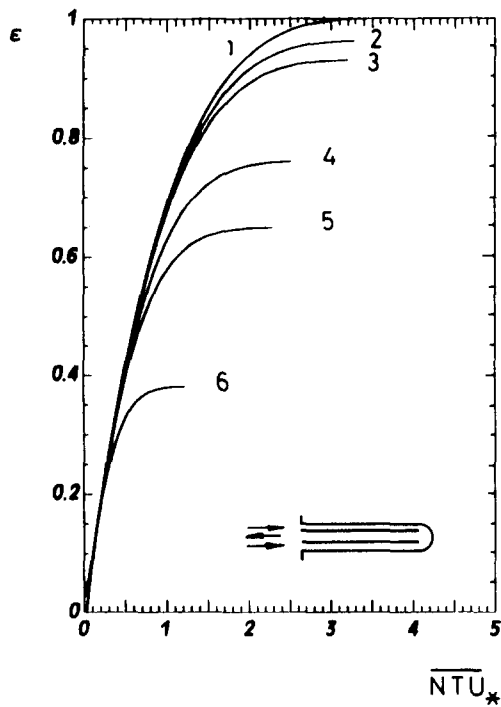


Figure 15 Condenser effectiveness for flow arrangement B. \overline{Hu} : (1) 0.0, (2) 0.05, (3) 0.1, (4) 0.5, (5) 1.0, (6) 5.0

Figure 15 *Efficacité du condenseur pour l'écoulement B. Hu : (1) 0.0, (2) 0.05, (3) 0.1, (4) 0.5, (5) 1.0, (6) 5.0*

To illustrate the consequence of variable heat-transfer coefficient on the effectiveness, the energy equations, (1) and (2), may be solved by treating U_1 to be uniform for the entire flow length. Then the governing equations become linear. Together with the stated boundary conditions, an analytical solution to the temperature distribution may be obtained. Such a solution neglects the effect of the flow arrangement and reveals that the effectiveness is only a function of two parameters defined respectively as, $NTU_a = U_1 A_{o1} / \dot{m} c_p$ and $Hu_a = ntu / NTU_a$. Therefore, in comparing the results of the present findings with the analytical solution, these two parameters should be identical to the corresponding ones of the present study. Figure 16 may be observed in this respect. In this figure, for the flow arrangement A, the Hurd number is at unity, and the numerically calculated effectiveness of the evaporator and the condenser are compared with the analytical solution. Disregarding the fundamental distinction in the heat-transfer mechanisms, the analytical solution provides the same effectiveness-curve for both the evaporator and the condenser and deviates considerably from the numerical results. In Figure 16 at $NTU^* = 2.0$, the analytical solution overestimates the evaporator effectiveness by 41.6% and underestimates the condenser effectiveness by 10.2%.

Concluding remarks

The numerical method of solution proposed in this study sheds light on the thermal design of the bayonet-tube heat exchanger for the shell-side fluid in evaporating or in condensing conditions. The wall superheat on the tube surface is assumed to vary in a range so that the nucleate boiling regime is always maintained. For the condenser case, laminar film condensation is assumed to exist on

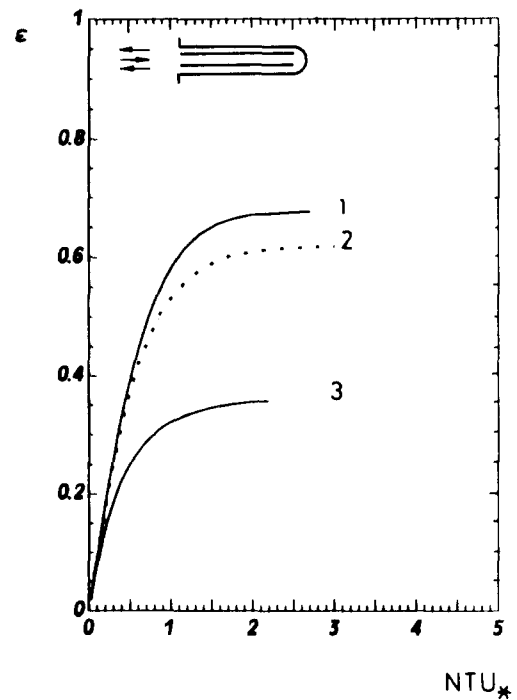


Figure 16 Comparison of the present study effectiveness results with the uniform film coefficient solution at $Hu = 1$. The flow arrangement type is A. (1) condenser, (2) solution for the uniform film coefficient, (3) evaporator

Figure 16 *Comparison des résultats d'efficacité de la présente étude avec la méthode du coefficient de film uniforme avec $Hu = 1$. Pour l'écoulement de type A. (1) condenseur; (2) solution pour le coefficient du film uniforme; (3) évaporateur*

the outer surface of horizontally oriented tubes. The governing equations, (15), (16), (37) and (38), are driven for a constant temperature, T_s , of the shell-side fluid. Therefore, the present solution method is applicable only to the evaporators and the condensers for pure fluids.

In the analysis, varying the thermal resistance ratio, ζ , in the range of 10^{-5} and 10^{-1} , the corresponding NTU^* values are computed by an iterative method of solution of the governing equations at a particular Hu number. The increment size ΔX is assumed to be constant at 0.001 for the entire analysis. This assumption causes a maximum computational error of 3.5% for the smallest NTU^* value of 0.028 and is considered to represent adequately the thermal behaviour of the exchanger. Scanning all the outlet temperatures, a smallest value of 0.01 is noted for the condenser case in the reverse flow arrangement. Thus, in regard to the energy balance condition; $|\theta_{p_{new}} - \theta_{p_{old}}|_{j=1} < 5 \times 10^{-4}$, the maximum computational error caused in estimating the exchanger outlet temperature is $\pm 5\%$. Referring to Equation (46), the exchanger effectiveness is also subject to the same error as the outlet temperature. Thus the computed effectiveness possesses a maximum of 5% error.

For flow entering the inner tube, at high values of Hu -number, $Hu \geq 0.5$, the temperature distribution exhibits a minimum. Depending upon the Hurd number, the minimum temperature varies in the range from 0.832 to 0.48 for the evaporator, and between 0.76 and 0.09 for the condenser. As Hu increases, the minimum temperature point moves toward the tube-tip.

In addition to the parameters of Hu and NTU^* , the exchanger effectiveness depends upon the flow

arrangement. At identical design conditions, the evaporator with the flow entering the annulus is determined to perform better than when flow enters the inner tube. However, the opposite is true of the condenser case. In all cases, an increase in Hu number causes a decrease in the exchanger effectiveness.

Acknowledgement

The author would like to acknowledge the financial assistance provided by the University Research Funds under the grant no. 0908.93.07.06.

References

- 1 **Kern, D. Q.** *Process Heat Transfer* 23rd edn, McGraw-Hill, London, (1986) 738-746
- 2 **Hurd, N. L.** Mean temperature difference in the field of bayonet tube *Indus Engng Chem* (1946) **38** 1266-1271
- 3 **Chung, H. L.** Analytical solution of the heat transfer equation for a bayonet tube exchanger *ASME Winter Annual Meeting* no. 81-WA/NE-3 (1981)
- 4 **Chung, H. L.** Effect of radiation heat transfer on a bayonet tube heat exchanger. *AIChE J* (1986) **32** 341-343
- 5 **Mathur, A., Saxena, S. C., Qureshi, Z. H.** Heat transfer to a bayonet heat exchanger immersed in a gas-fluidized bed. *Int Comm Heat Mass Transfer* (1983) **10** 241-252
- 6 **Luu, M., Grant, K. W.** Thermal and fluid design of a ceramic bayonet tube heat exchanger for high temperature waste heat recovery *Proceedings - Symposium on Industrial Heat Exchanger Technology* (1985) 159-173
- 7 **Kakaç, S., Shah, R. K., Aung, W.** *Handbook of Single-phase Convective Heat Transfer* Wiley, New York (1987) chaps. 3 and 4
- 8 **TEMA Standards of the Tubular Exchanger Manufacturers Association 7th edn** Tubular Exchanger Manufacturers Association, New York (1988) 208-215
- 9 **Rohsenow, W. R., Hartnett, J. P.** *Handbook of Heat Transfer* McGraw Hill, New York (1973) section 13
- 10 **Kayansayan, N.** Mean heat flux concept in evaporator design *Int J Refrig* (1988) **11** 46-51
- 11 **Carnahan, B., Luther, H. A., Wilkes, J. O.** *Applied Numerical Methods* Wiley, New York (1969) 341-365
- 12 **Collier, J. G.** *Convective Boiling and Condensation* 2nd edn, McGraw-Hill, New York (1972) chap. 10